Persistence Lengths and Structure Factors of Wormlike Polymers under Confinement

Peter Cifra,* Zuzana Benková, and Tomáš Bleha

Polymer Institute, Slovak Academy of Sciences, Dúbravská cesta 9, 842 36 Bratislava, Slovakia

Received: August 8, 2007; In Final Form: November 7, 2007

The behavior of semiflexible chains modeling wormlike polymers such as DNA and actin in confined spaces was explored by coarse-grained Monte Carlo simulations. The persistence length P, mean end-to-end distance $\langle R^2 \rangle$, mean radius of gyration $\langle R_g^2 \rangle$, and the size ratio $\langle R^2 \rangle / \langle R_g^2 \rangle$ were computed for chains in slits, cylinders, and spheres. It was found that the intrinsic persistence length of a free chain undergoes on confinement substantial alteration into the apparent persistence length. The qualitative differences were found in trends of the apparent persistence lengths between slits and cylinders on one side and spheres on the other side. The quantities P, $\langle R^2 \rangle$, $\langle R_g^2 \rangle$, and $\langle R^2 \rangle / \langle R_g^2 \rangle$ display similar dependences upon squeezing the chains in nanopores. The above quantities change nonmonotonically with confinement in slits and cylinders, whereas they drop smoothly with decreasing radius of a sphere. For elongation of a chain in a cylinder, two regimes corresponding to strong and moderate confinements were found and compared to experiments and predictions of the blob and Odijk theories. In a spherical cavity, the toroidal chain structure with a hole in the center was detected under strong confinements. The scattering form factor $S(q)$ computed for semiflexible confined chains revealed three regimes of behavior in a slit and a cylinder that matched up well with the scaling theory. The complex form of the function $S(q)$ computed for a sphere was interpreted as a sign of the toroidal structure. A reasonable agreement was found between the simulations and measurements of DNA and actin filaments, confined in nano- and microfluidic channels and spherical droplets, pertaining to the changes of the persistence lengths, chain elongation, and toroidal structure formation.

Introduction

There has been a long-standing interest in the subject of confined polymers because of its relevance to numerous biological processes. Confinement of a protein into a roughly spherical or cylindrical cavity is presumed to significantly stabilize the folded state of a protein.[1] Lately, investigations of biopolymer confinement are inspired by the advances in photolitography techniques that allow fabrication of well-defined nano- and microchannels. Chip-based microfluidic devices in combination with fluorescence microscopy are used to manipulate, observe, and characterize stiff polymers such as DNA and actin.[2−5] It is hoped that by this technique DNA can not only be separated by size but actually sequenced at the single-molecule level.

The model of wormlike chains (WLCs) has been widely used to provide fundamental understanding of the properties of stiff synthetic and biological polymers. The WLC model describes the polymer of fixed contour length L_c as a string of constant bending elasticity. The energy in the standard (ideal) WLC model is given just by the energy due to chain curvature, and the self-avoidance of segments is ignored. The persistence length P, the characteristic length of tangent−tangent orientation correlations of segments along the chain, serves as a quantitative measure of the chain stiffness in semiflexible chains.

There are several means[6,7] to define the persistence length P of a macromolecular chain: (a) P is given by the average projection of the end-to-end vector on the tangent to the chain contour at a chain end for infinitely long chains (IUPAC definition), (b) P is determined from the exponential decay of orientation correlation in a chain, (c) P is computed from the average cosine of the bond angle in a chain, and (d) P is computed from the formula derived for the WLC model relating the mean-square end-to-end distance of a chain $\langle R^2 \rangle$ to its persistence length. In unconfined systems, the value of P may slightly differ according to definitions (a−d).[7] Method a, the most general computational approach, seems to be best suited also for application to confined polymers. Methods b and d underlie the determination of the persistence length P in solution or in bulk by a variety of experimental methods such as atomic force microscopy, viscosity, flow birefringence, and radiation scattering.[8]

The persistence lengths extracted from measurements are often the apparent values involving the external contributions due to temperature, solvent quality, polymer concentration, electrostatic interaction, presence of ions, and so forth, that contribute to the intrinsic chain stiffness. There are indications from experiments,[4,5] simulations,[9,10] and theory[11] that confinement can be an important external factor potentially affecting the intrinsic persistence length. In a study of the change of molecular properties upon confinement, the actin filaments serve as a very convenient experimental model of stiff biopolymers. The persistence length P measured for actin confined to a rectangular channel was found[4,5] to considerably increase on reduction of the channel width. Simulations modeling the confined actin filaments[9] revealed that the persistence length of a quasi-two-dimensional chain in a narrow slit can be twice of the value of P in bulk. In contrast, simulations of chains in spherical cavities[10] predict that confinement prevents the persistence length of an encased chain to develop to the value found in a free chain. Clearly, a thorough examination of the confinement effect on P in various restricted geometries such as slits, tubes, and spheres is needed.

10.1021/jp076355n CCC: $40.75
Published on Web 01/15/2008

Confining geometries with purely repulsive walls modify natural size and shape of polymer chains, their orientation, and Brownian dynamics. As a result, the other dimensional characteristics of chains such as the mean end-to-end distance R or the mean radius of gyration R_g should be potentially affected by confinement in a way similar to that of the persistence length. For example stiff chains confined in cylindrical nanochannels are extended to a substantial fraction of their contour length.[3,4] In general, the chain stiffness, the geometry, and the strength of confinement control the shape and global dimensions of a chain. Three competing length scales affect the final structure of a confined chain: (a) the mean end-to-end distance R (or the contour length L_c), (b) the persistence length P, and (c) the confinement scale length D, given as the half-width of a slit and the radius of a cylinder or a sphere. For flexible self-avoiding polymers, a nonmonotonic function of R versus D is well ascertained in slitlike and cylindrical pores from simulations and analytical calculations.[12−15] On reduction of D, the mean chain elongation R in slits and cylinders at first decreases from the value for a free chain ($D \rightarrow \infty$), then goes through a minimum, and, finally, distinctly increases as the chain is strongly squeezed.

In semiflexible polymers, the analysis of chain elongation was focused on chains in a cylinder. When the cylinder width $2D$ is larger than the persistence length, the blob model of polymers predicts[16] that the equilibrium mean end-to-end distance R in a channel scales with $D^{-2/3}$. On the other hand, in the strong confinement limit $2D \ll P$, a new length scale, the deflection length $\lambda = (4D^2P)^{1/3}$, was introduced.[11] In this Odijk regime, the mean end-to-end distance R should change with $-D^{2/3}$.

Several experiments employing fluidic nanochannels fabricated by chip lithography were conducted on stiff chains in order to understand the mechanism of their elongation. Tegenfeldt et al.[17] have extended DNA molecules in imprinted nanochannels and found the linear dependence of the polymer extension with the genomic length. Chen et al.[2] investigated the uniaxial (slit) and biaxial (square channel) confinement of DNA and found that the chain stretching followed the scaling (blob) predictions. Reisner et al.[3] addressed a similar problem under the condition that the persistence length of DNA is of the same order as the channel width and found evidence for the crossover between the blob and Odijk regimes. In a related study of actin in rectangular microchannels, almost fully stretched actin filaments were visualized in narrow pores.[4] Odijk deflection length λ was determined as a function of the channel width, and its variation with $D^{2/3}$ was verified.[4]

In a spherical cavity, the absence of leeway for a chain to escape the confinement brings a striking difference in chain properties under 3D confinement in sphere relative to 2D and 1D restrictions in a cylinder and a slit, respectively. The model of spherical confinement is highly relevant to various biological caging of macromolecules in a roughly spherical volume such as proteins in pores[1] or DNA packaging in a virus.[18] The key question to answer is how the chain can be confined in dimensions radically smaller than its contour length and comparable to (or smaller than) its intrinsic persistence length. In flexible polymers, squeezing of a chain in a spherical cavity should result in formation of a random globule. In semiflexible chains, the globularization process may compete with formations of the folded structures and hairpins, or alternatively, the toroidal structure of a chain aligned along the internal wall of a sphere can be spontaneously formed.[18]

Monte Carlo (MC) simulation is a powerful tool to clarify the unresolved questions of the static and dynamic response of semiflexible polymers to confinement. Apart from persistence length and the mean end-to-end distance R, essential characterization of internal structure of confined molecules can be obtained from the single-chain structure factor. The static structure factor $S(q)$ is a valuable quantity readily available from light and neutron scattering techniques. The MC computations of structure factor offer deeper insight into changes of the chain structure and organization as a function of the strength and the geometry of confinement.

In the present paper, we utilize the MC simulations of the discretized coarse-grained, WLC model to calculate the persistence length, the chain dimensions, and the structure factors of polymers confined in three representative constraining geometries: a slit, a cylinder, and a sphere. The chain stiffness considered in simulations should cover the linear macromolecules from flexible to rather stiff synthetic and biological polymers. We report the transformations of the intrinsic persistence length into the apparent one on confinement. We find the qualitative differences in the trends of apparent persistence length and the chain dimensions between slits and cylinders on one side and spheres on the other side. For chain elongation in a cylinder, we validate the crossover between the blob and Odijk regimes. In a spherical cavity, the toroidal chain structure with a hole in the center is found under strong confinements. The very rich structure observed in the computed form factors of confined chains is rationalized by the scaling theory arguments.

Simulation Model

We have used a hybrid coarse-grained model of semiflexible chains described in previous papers aimed at threading of chains between interconnected cavities[10] and elasticity of stiff macromolecules.[19] A chain in the model consists of bead units connected by effective bonds characterized by stiff springs. Each effective bond represents several chemical bonds along the chain backbone. An effective bond is described by finitely extensible nonlinear elastic potential (FENE)[20]

$$U_{\mathrm{FENE}}(l) = -\kappa r^2 \ln\left[1 - \left(\frac{l - l_0}{\mathrm{r}}\right)^2\right] \qquad (1)$$

The bond stretching is considered to be temperature independent, $\kappa/kT = 20$. The bond length l in the potential varies around the preferred distance $l_0 = 0.7$ and $r = l_{\max} - l_0$. The contour length of a chain is $L_c = (N - 1)\langle l\rangle$, where $\langle l\rangle$ is the average length of effective bonds. In contrast to the constant L_c assumed in the standard WLC model, eq 1 introduces fluctuations of the contour length into the model.

Variation of chain stiffness is expressed by the bending potential[21] between two consecutive bonds in the chain backbone

$$U_b = b^*(1 + \cos\theta_i) \qquad (2)$$

where θ_i is a valence angle and the stiffness parameter (the bending force constant) $b^* = A\epsilon$ is proportional to the pair contact interaction energy. Further on we will use the reduced stiffness parameter, $b = b^*/kT$.

A Morse-type potential[20] is used for the nonbonded interactions between effective monomeric units (beads) separated by distance r. The potential includes a quasi-hard-core self-avoidance and an attraction part

$$U_M(r)/\epsilon = \exp[-2\alpha(r - r_{min})] - 2\exp[-\alpha(r - r_{min})] \quad (3)$$

where $\alpha = 24$ and the minimum of the potential $r_{min} = 1.14l_0$ was selected. This short-range potential predicts negligible interaction at $r \geq 1$ and the core radius of a bead around $\sigma \approx 0.54l_0$.

The principal parameters of the model are the pair interaction energy ϵ and the chain stiffness b (related to the persistence length P). When the temperature is expressed in units of the Boltzmann constant k and the attractive potential of the unit strength $\epsilon/k = 1$ is chosen, simulations correspond to the temperature $T = 1$, well above the Θ state located at temperature of about $\Theta \approx 0.62$ for flexible chains.[20] Incorporation of self-interaction of beads introduces the excluded volume (EV) effect into the model. Previous analysis using this model revealed[19] that the influence of EV on chain properties rapidly diminished with an increase of chain stiffness and turned negligible for the stiffness parameter $b > 5$.

Three types of hard-wall confining geometry, a slit, a cylinder, and a sphere, were considered. The strength of confinement is determined by the characteristic dimension D^* of a pore, where D^* stands for the half-width in a slit and for the radius in a cylinder and a sphere. Centers of beads are not allowed to go beyond these limits. To account for overall volume available for beads, the distance $D = D^* + \sigma$ is used henceforth to specify the confinement. The periodic boundary conditions were assumed along the axes parallel to the slit plates in the case of uniaxial confinement and along the long axis of a cylinder in the case of biaxial confinement.

The Metropolis MC method with reptation and kink jump chain updates was used to obtain the ensemble averages. For strong confinement in a spherical cavity, we had to use a special technique to build the initial configuration of a dense globule in the cavity with volume fraction φ up to 0.4. The initial configuration was built by chain growing. After a segment was added to the growing chain, a series of the kink jumps of previously added segments was performed in order to accommodate successfully the whole chain into the cavity. A bias introduced by this insertion was removed by equilibration after the whole chain was grown, prior to collecting the ensemble averages. Presented results correspond to the chain length N of 200 beads. Up to 3×10^7 MC cycles of trial moves was used in chain generation. The error estimates of ensemble averages are mostly within the size of symbols in the figures. The distribution functions of the end-to-end distances $P(R)$ and of the radius of gyration $P(R_g)$ were evaluated by grouping the values of R and R_g from simulations into a histogram. The mean end-to-end distance $R = \langle R^2\rangle^{1/2}$ and the mean radius of gyration $R_g = \langle R_g^2\rangle^{1/2}$ were computed by a standard procedure. Throughout this paper, the chain dimensions and other length parameters are normalized by the unit bond length $l_0 = 0.7$. The stiffness of simulated chains varied from fully flexible chains ($b = 0$) as the reference point to moderately stiff chains ($b = 20$) resembling biopolymers such as DNA.

Results and Discussion

Chain Stiffness in Slits and Cylinders. The persistence length P was computed from the rigorous definition,[6,7] as the average sum of all bond vector projections (or the end-to-end vector projection) on the first bond of a chain and extrapolation to infinitely long chains $N \rightarrow \infty$ ($P = P_\infty$)

$$P = \langle \sum_{i=1}^{N-1} \mathbf{l}_i\mathbf{l}_1\rangle/\langle l\rangle = \langle \mathbf{R}\mathbf{l}_1\rangle/\langle l\rangle \quad (4)$$

For the considered range of the stiffness parameter b from 0 to 20, it was found in an earlier study[19] that the chain length $N = 200$ is already sufficient to reach the limiting value of P_∞.

In the continuous WLC model, a direct proportionality between the bending force constant b and persistence length P was deduced from the elasticity theory of flexible rods

$$b = P/\langle l\rangle \quad (5)$$

Validity of such a linear relation for the present discrete WLC model was confirmed[19] in case of unconfined chains of stiffness $b > 5$. Alternatively to the parameter b, the chain stiffness is conveniently judged by the ratio of two experimentally accessible quantities, of the contour and persistence lengths L_c/P. By introduction of the mentioned model parameters we can map the model to the real polymers: for a typical stiff DNA macromolecule we have $2\sigma \approx \langle l\rangle = 2.5$ nm (7.4 base pairs) and $b = P/\langle l\rangle = 50$ nm (147 bp)/2.5 nm $= 20$, the value of stiffness used in the results below.

At first, the semilogarithmic plot of the dimensionless persistence length P of chains in a slit and cylinder, respectively, is presented in Figure 1 for chain stiffness $b = 5$ and $b = 20$ as a function of a pore dimension D. As $D \rightarrow \infty$ the pore has no effect on the persistence length and the value of $P = P_{3D} = 19.8$ of a free chain in 3D is retrieved. On reduction of D, the persistence length at first slightly decreases, and then, at the pore dimension D near to R_g the curves go through a shallow minimum in both confining geometries. The minimum is more pronounced in a cylinder than in a slit and is shifted to higher D in stiffer chains. Finally, the persistence length increases at strong chain squeezing; the rate of this upturn in P differs considerably for a slit and a cylinder. As $D \rightarrow 0$ the confinement induces low-dimensional anisotropy of polymer conformations that is much stronger in a cylinder, where the chain can be stretched only in one dimension. From the two types of chains shown in Figure 1 in a cylinder, the more flexible chain of $b = 5$ is more drastically affected by confinement.

The persistence length of a free chain P_{3D}, a quantity accessible by measurements and/or computations, can be related to the characteristic ratio, $C_\infty = \langle R^2\rangle/nl^2$, or the Kuhn segment length l_K, employed frequently in the flexible chain models. However, the bulk persistence length P_{3D} has to be differentiated from the apparent persistence lengths characterizing chains at uni- or biaxial confinement that can be extracted from plots in Figure 1 in the region of very narrow pores. The ratio of the apparent and intrinsic persistence lengths P_{2D}/P_{3D} in a slit and P_{1D}/P_{3D} in a cylinder as a function of the confinement distance D for a chain of $N = 200$ is given in Table 1. For example, the ratio P_{2D}/P_{3D} and P_{1D}/P_{3D} is 1.26 and 4.26, respectively, at $D = 7.7$ and the stiffness parameter $b = 20$. For the hypothetical situation $D \rightarrow 0$, the linear extrapolation of data in Figure 1 gives $P_{2D}/P_{3D} = 1.87$ and $P_{1D}/P_{3D} = 9.10$ for a chain of $b = 20$. As a result, the persistence length P_{1d} in the cylinder at $D \rightarrow 0$ is 4.87 times larger than P_{2D} in the slit. The value 1.87 computed for the ratio P_{2D}/P_{3D} is in accord with the previous finding[9] that this ratio changes as a function of the bending parameter from 1 to the limiting value of 2 for stiff chains. Similar computations for other values of b show that P_{2D}/P_{3D} at $D \rightarrow 0$ should always be smaller than the corresponding P_{1D}/P_{3D}.

Predictably, both the intrinsic and apparent persistence lengths increase with the chain stiffness. The rate of this increase in

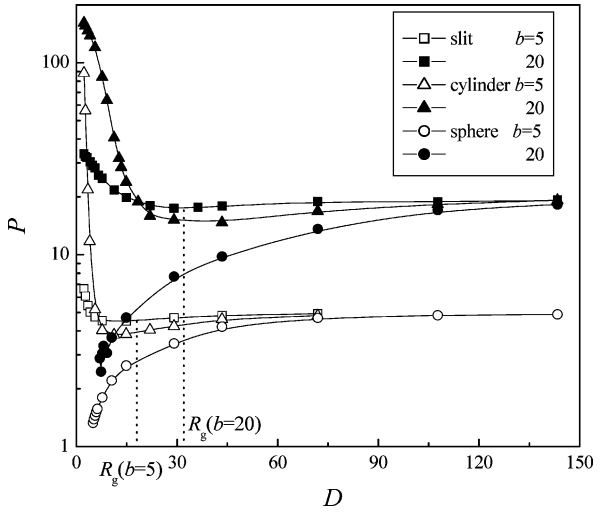

Figure 1. Semilogarithmic plot of the apparent persistence length of a confined chain $N = 200$ and the stiffness parameter $b = 5$ and 20 as a function of the uni-, bi-, and triaxial confinements defined by D, the half-width of a slit and the radius of a cylinder or sphere, showing strong effect of confining geometry. The values of the mean radius of gyration of a free chain of $b = 5$ and 20 are indicated by dotted lines.

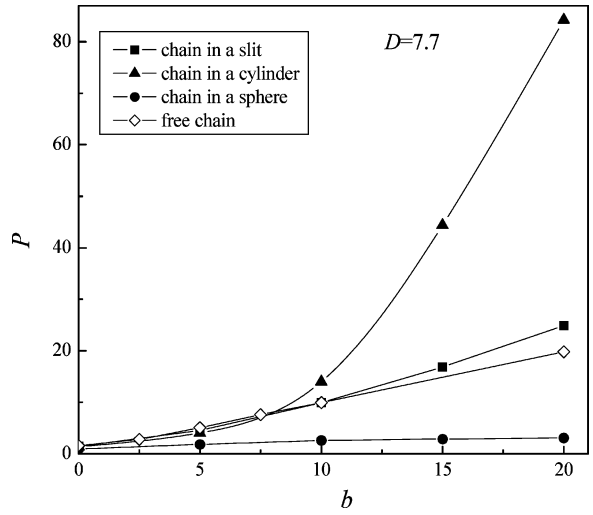

Figure 2. Variation of the apparent persistence length with the stiffness parameter for a chain confined in a slit with half-width D, in cylinder and sphere with radius D and for a free chain.

confined chains relative to a free chain depends on the pore size considered. The situation for $D = 7.7$ is illustrated in Figure 2. The linear relationship between the persistence length and the stiffness parameter b found for a free chain in Figure 2 validates eq 5. In confined chains, the dependence P versus b becomes more complex.

The simulation results presented suggest that the confinement-induced changes of the persistence length P can be substantial in narrow pores, particularly in a cylinder. These confinement effects may be comparable or even stronger than other major contributions to the intrinsic chain stiffness such as the "electrostatic" stiffness due to Coulombic repulsion between like charges along the chain (and its modification by the presence of counterions) or the "topological" stiffness due to side groups in comb or branched polymers.

The experimental results on alteration of the persistence length by confinement are very sparse and concern mainly actin filaments. Two-stranded helical filaments of F-actin with a diameter of about 8 nm assemble from globular actin monomers (G-actin). Actin filaments are semiflexible polymers on the

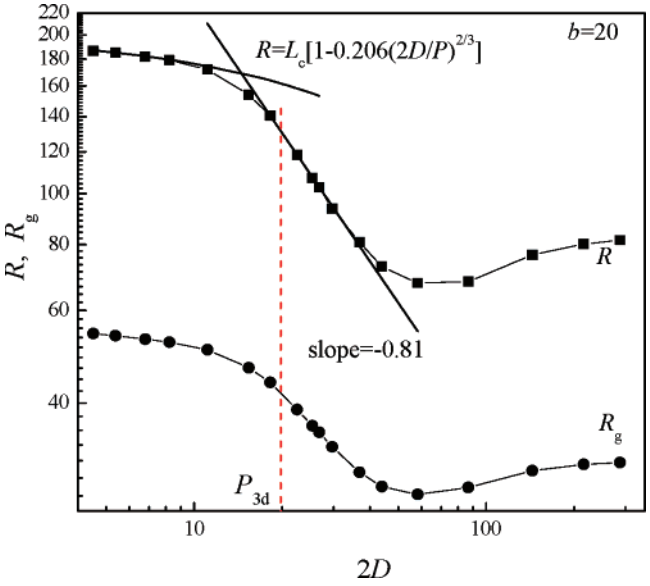

Figure 3. Logarithmic plot of the mean end-to-end distance $R = \langle R^2 \rangle^{1/2}$ and the mean radius of gyration $R_g = \langle R_g^2 \rangle^{1/2}$ of a confined chain with stiffness parameter $b = 20$ as a function of the cylinder diameter showing the transition from weak to strong confinement regime. The inserted equation relates R to $2D$ in the Odijk regime, and the slope indicates the scaling relation in de Gennes regime.

micrometer scale, and thus, they can be visualized by video fluorescence spectroscopy. In unconfined actin filaments, the persistence length P_{3D} is of the same order as the contour length and lies in a broad interval 4−20 μm. Very recently, the apparent persistence length P of actin in rectangular channels was determined[5] from the exponential decay of orientation correlation in a chain. The depth of channel was constant (1 μm), and the channel width varied from 20 to 3 μm. The persistence length $P = 5.9$ μm determined in the wide channels is similar to a value $P_{2D} = 7.4 \pm 0.2$ μm extracted from other experiments[22] of actin confined in a slit. However, by decreasing channel width from 20 to 3 μm a striking increase of P from 5.9 to 38.2 μm was recorded in the experiment.[5] Such an increase of the apparent persistence length measured in rectangular channels resembles the increase in P of a chain in a cylinder shown in Figure 1.

The variation of the persistence length of semiflexible chains with the cylinder radius D (Figure 1) displays the pattern well-established for the dependence of the mean end-to-end distance $R = \langle R^2 \rangle^{1/2}$ and the mean radius of gyration $R_g = \langle R_g^2 \rangle^{1/2}$ on D in flexible polymers.[12−15] The nonmonotonic form of these curves is conserved also in semiflexible polymers as seen in Figure 3 on the logarithmic plots of R versus $2D$ and R_g versus $2D$ in a cylinder. The function $R(2D)$ goes through a minimum located at about $2R_g$, and then chain elongation increases on stronger chain squeezing. A similar, albeit a less pronounced, pattern of such curves was also computed for a semiflexible chain in a slit (not shown).

Modification of the chain shape by confinement is illustrated by the changes of the size ratio $\langle R^2 \rangle / \langle R_g^2 \rangle$ in nanopores of various geometry presented in detail in Table 2. For pore size larger than the contour length L_c, the influence of confinement is negligible and the size ratio is around 7 and 6.3 for a chain of $b = 20$ (Figure 4) and $b = 0$ (Tab. 2), respectively. The corresponding value from the theory for flexible EV chain in bulk reads 6.303.[23] In a slit at $D \rightarrow 0$, the size ratio is about 8.1 and 7.1 for a chain of $b = 20$ (Figure 4) and $b = 0$ (Table 2), respectively. The latter value is close to the ratio 7.15 for a 2D flexible EV chain.[24] The size ratio 6 applies to the ideal 2D

TABLE 1: Ratio of the Apparent and Intrinsic Persistence Lengths for a Chain of $N = 200$ and the Stiffness Parameter b in Uni-, Bi-, and Triaxial Confinements Defined by D, the Half-Width for a Slit and the Radius for a Cylinder and a Sphere

	slit P_{2D}/P_{3D}[a]			cylinder P_{1D}/P_{3D}[a]			sphere P_{sph}/P_{3D}[a]		
D	$b = 0$	$b = 5$	$b = 20$	$b = 0$	$b = 5$	$b = 20$	$b = 0$	$b = 5$	$b = 20$
2.26	1.06	1.32	1.69		17.53	8.15			
2.69	1.00	1.21	1.64		11.19	7.86			
5.54	0.95	0.94	1.42	0.93	1.03	6.05	0.49	0.29	
7.69	0.94	0.90	1.26	0.87	0.80	4.26	0.60	0.36	0.15
14.83	0.96	0.89	1.00	0.89	0.76	1.21	0.79	0.52	0.24
29.11	0.99	0.93	0.88	0.96	0.84	0.77	0.92	0.68	0.39
43.40	1.00	0.96	0.90	0.98	0.92	0.74	0.96	0.84	0.49
71.97	1.00	0.98	0.95	0.99	0.96	0.85	0.99	0.93	0.69

[a] The persistence lengths of a free chain P_{3D} are 1.56, 5.03, and 19.79 for $b = 0$, $b = 5$, and $b = 20$, respectively.

TABLE 2: Size Ratio $\langle R^2\rangle/\langle R_g^2\rangle$ for a Chain of $N = 200$ and the Stiffness Parameter b in Uni-, Bi-, and Triaxial Confinements Defined by D, the Half-Width for a Slit and the Radius for a Cylinder and a Sphere

	slit[a]			cylinder[a]			sphere[a]		
D	$b = 0$	$b = 5$	$b = 20$	$b = 0$	$b = 5$	$b = 20$	$b = 0$	$b = 5$	$b = 20$
2.26	7.07	6.82	8.01		11.51	11.84			
2.69	7.01	6.71	7.91		10.95	11.83			
5.54	6.61	6.48	7.84	8.37	7.79	11.59	2.35	2.26	
7.69	6.33	6.33	7.66	6.93	6.94	10.88	2.60	2.41	2.27
14.83	6.04	6.04	7.22	5.48	5.65	8.01	3.74	2.94	2.35
29.11	6.22	6.02	6.76	6.03	5.48	6.35	5.67	4.37	3.07
43.40	6.28	6.14	6.75	6.19	5.893	6.05	6.05	5.41	3.92
71.97	6.30	6.21	6.96	6.26	6.13	6.58	6.21	5.96	5.78

[a] The $\langle R^2\rangle/\langle R_g^2\rangle$ values for a free 3D, 2D, and 1D flexible EV chain are 6.303, 7.15, and 12, respectively.

and 3D chains. The chain in a cylinder under strong squeezing becomes rodlike, and the ratio $\langle R^2\rangle/\langle R_g^2\rangle$ approaches the rigid rod limit of 12 (Figure 4). A snapshot of such a stretched conformation of a chain of $b = 20$ in a very narrow cylinder is shown in Figure 5. At this confinement, the chain is extended to 90% of its contour length. Overall, the anisotropy of confined molecules inferred from the size ratio is in qualitative accord with the computed dependences $P(D)$, $R(D)$, and $R_g(D)$. As shown in Figure 4, the $\langle R^2\rangle/\langle R_g^2\rangle$ values approach the limiting values at $D \to 0$ through a flat minimum which is slightly more significant for a chain in a cylinder than for a chain in a slit. The minimum is located around the mean radius of gyration of a free chain. It is worth noticing in Table 2 that the largest size ratios are calculated for semiflexible chains of $b = 20$ while, with a few exceptions, chains of $b = 5$ tend to display the smallest size ratios.

The dependence R versus $2D$ from simulation in a cylinder is compared in Figure 3 with two theoretical models employed in rationalization of the mean chain elongation in a cylinder. The de Gennes blob model applies when the cylinder width $2D$ is larger than (or at most comparable to) the free-chain persistence length P_{3D}. Self-avoidance divides the confined polymer into a linear series of noninterpenetrating blobs. As a result, the mean end-to-end distance R scales[16] linearly with the contour length and as $D^{-2/3}$ with the cylinder radius D

$$R \approx L_c P^{1/3} D^{-2/3} \tag{6}$$

On the other hand, a new variable, the deflection length $\lambda = (4D^2P)^{1/3}$, is crucial in the strong confinement regime, $2D < P_{3D}$.[11] Deflections made by the polymers with the cylinder walls occur over the length λ on average; the chain is extremely stiff on the scale of λ. This intuitively appealing picture of chain deflections in narrow pores is exemplified in a snapshot in Figure 5 though neither the snapshot nor the scattering function (see below) show indication of very regular deflections from the wall. In this regime, the mean end-to-end distance R is[11]

$$R \cong L_c[1 - A(2D/P)^{2/3}] \tag{7}$$

where A is a constant.

Both regimes described by eqs 6 and 7 can actually be seen in the data for the mean chain elongation in a cylinder plotted in Figure 3 for a chain of $b = 20$. Simulation data in the blob regime at moderate confinements can be fitted by the slope -0.81 which is somewhat larger than $-2/3$ predicted by eq 6. In narrow pores, the data are matched by eq 7 when constant $A = 0.206$ is used in eq 7. The crossover between the blob and Odijk regimes occurs in Figure 3 around $2D = 15$, somewhat below the prediction, $2D \sim P_{3D} = 19.8$ indicated by the vertical line.

In the experimental paper,[3] well-defined rectangular channels combined with molecular imaging were used to explore the biaxial confinement of DNA. The mean end-to-end elongation of DNA was measured[3] as a function of D_{av} (geometrical average of the channel width and depth). Similarly to simulations in Figure 3, the two kinds of regimes were observed[3] on the logarithmic plot of the function $R(D_{av})$. Consistently with our findings, the exponent -0.85 in eq 6 determined from measurements in the blob regime exceeded $-2/3$. By using the constant $A = 0.361$ in eq 7, the crossover to the Odijk regime was located[3] at $D_{av} = 110$ nm, which is at about twice the persistence length P of the unconfined DNA. In experimental studies of actin confined in rectangular microchannels, almost fully stretched filaments were visualized in narrow pores.[4,5] The Odijk deflection length λ was determined as a function of the channel width, and its variation with $\sim D^{2/3}$ confirmed.[4]

Computation of the entire distribution function of the end-to-end distance $P(R)$, instead of its mean value R only, reveals additional structural information about the effect of confinement. Figure 6 shows the function $P(R)$ of a chain of the stiffness

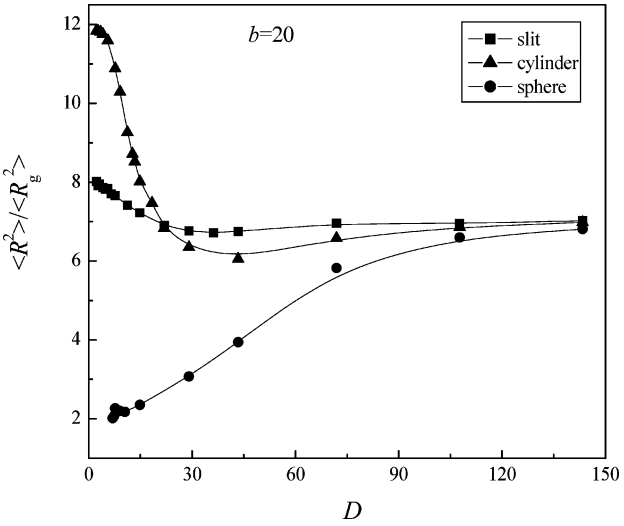

Figure 4. Variation of the size ratio for a confined chain of stiffness parameter $b = 20$ with the uni-, bi-, and triaxial confinements defined by D, the half-width of a slit and the radius of a cylinder or sphere.

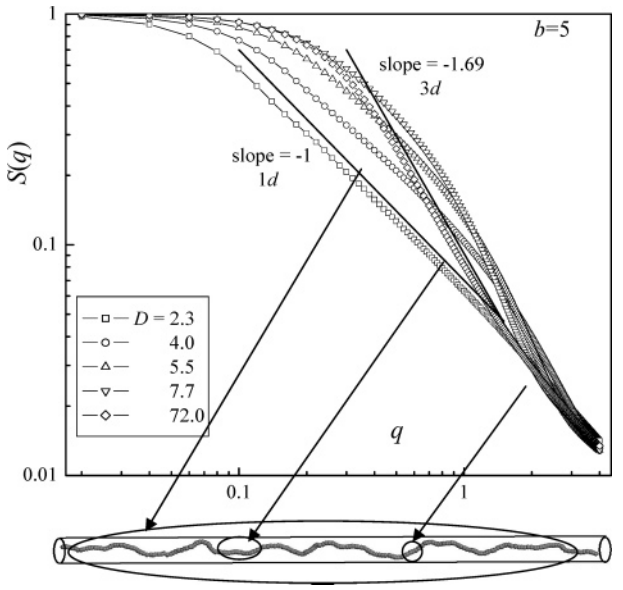

Figure 5. Logarithmic plot of the form factor of a chain with the stiffness parameter $b = 5$ confined in a cylinder of radius D given in the legend as a function of the scattering wavevector. Snapshot illustrates one chain conformation for $D = 4.1$, and the structure motifs are related to the behavior in particular ranges of the form factor.

parameter $b = 20$ squeezed in a cylinder. The initial fairly symmetrical distribution of a free chain narrows under mild squeezing of $D = 29.1$ ($\sim R_g$), and the maximum shifts to the left. On further compression in a cylinder, the second maximum starts to develop, and at $D = 13.4$ a bimodality of function $P(R)$ is clearly manifested. Evidently, two structures arise at this intermediate confinement, the hairpinlike bent chains with smaller R and the elongated chains with higher R. Unsymmetrical hairpins with subchains (legs) of unequal length may prevail in the bent structures. After crossover from the blob into the Odijk regime, the distribution function at strong confinement becomes again monomodal and its intensive peak moves toward the contour length (Figure 6).

Appearance of bimodality is a consequence of two opposite influences, confinement and chain rigidity. The hairpin structures can be locked as distinct entities only for stiff chains, and therefore, no bimodality was observed in more flexible chains of $b = 5$. In experiments with actin in rectangular channels,[4]

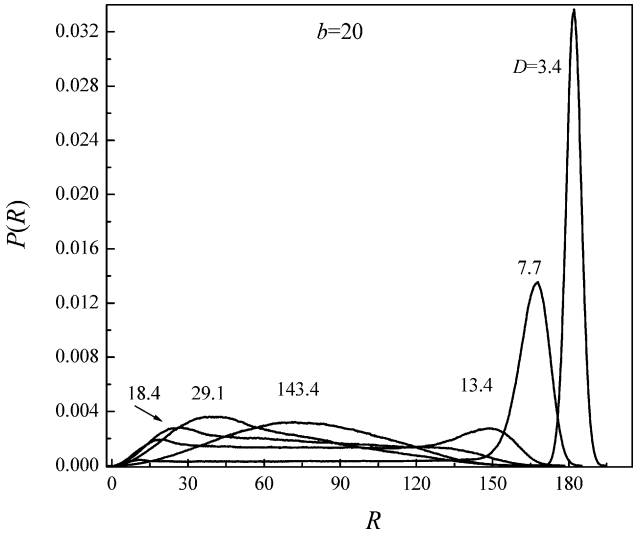

Figure 6. Radial distribution function of the end-to-end distance for a chain of stiffness parameter $b = 20$ confined in a cylinder with radius D. Bimodal distribution indicating hairpin formation is observed for $D = 13.4$.

the radial distribution function $P(R)$ of actin filaments was evaluated. In strongly confined chains, narrowing of the monomodal distribution and the shift of maximum to larger values of R were observed,[4] in harmony with the simulation data in Figure 6.

Chain Stiffness in a Sphere. In a spherical cavity, all three spatial dimensions limit the freedom of chains to escape the confinement. As a result, striking differences exist between the dimensional properties of chains in a sphere relative to those in a slit and a tube. For example, the persistence length of a chain in a sphere P_{sph} shows a monotonous decrease on compression of confining radius (Figure 1) for all stiffness parameters b considered. The dependence of persistence length P_{sph} on parameter b is much less steep than the equivalent function for an unconfined polymer (Figure 2); i.e., the persistence length of a spherically confined chain P_{sph} cannot develop to the extent found in a free chain P_{3D}.

Likewise, the trends in the changes of the mean end-to-end distance R and the mean radius of gyration R_g in a sphere are opposite to those in slits and tubes. The values of R and R_g of semiflexible chains are reduced by sphere compression, and this dependence is linear at small D (Figure 7). No scaling relation, pendant to eqs 6 and 7, is available for the mean end-to-end distance R of a chain confined in a sphere. In this context, it should be noted that the scaling relations for the confinement free energy in a sphere substantially differ from those for a slit and a cylinder.[25] Below $D < 14.8$, the compression is accompanied by the reduction of the effective mean bond length $\langle l \rangle$ and the mean valence angle $\langle \theta \rangle$ (Figure 8). Squeezing of a chain increases the polymer volume fraction φ inside the sphere; the high values of φ of about 0.4 can be achieved at small D (Figure 8).

Modification of the chain shape in a spherical cavity is further illustrated by the changes in the size ratio $\langle R^2 \rangle / \langle R_g^2 \rangle$ (Figure 4 and Table 2). Monotonous convergence of the size ratio to its limiting value at $D \rightarrow 0$ is seen. Contrary to the uni- and biaxial confinements, the size ratio of a spherically trapped chain decreases with increasing stiffness of a chain. Let us consider a fully compacted ($\varphi = 1$) ideal random chain in a sphere of radius D. The radius of gyration of a solid sphere is given as $R_g^2 = 0.6D^2$. The end-to-end distance of an ideal chain can be calculated as the average mean-square random distance within

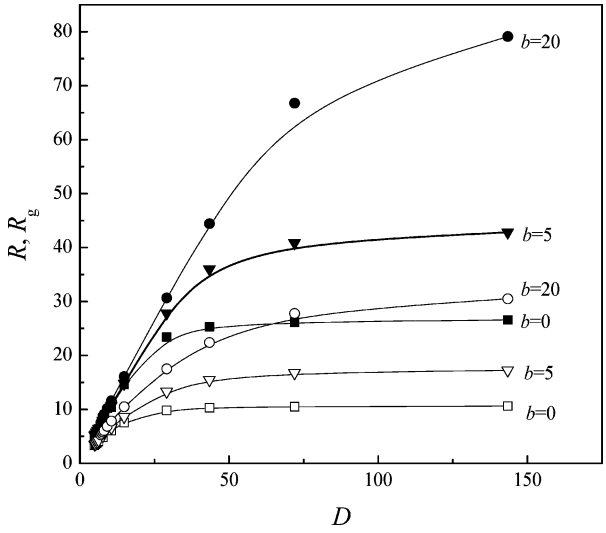

Figure 7. Variations of the mean end-to-end distance $R = \langle R^2 \rangle^{1/2}$ (solid symbols) and the mean radius of gyration $R_g = \langle R_g^2 \rangle^{1/2}$ (open symbols) with the sphere radius D for a confined chain of stiffness parameters $b = 0$, 5, and 20.

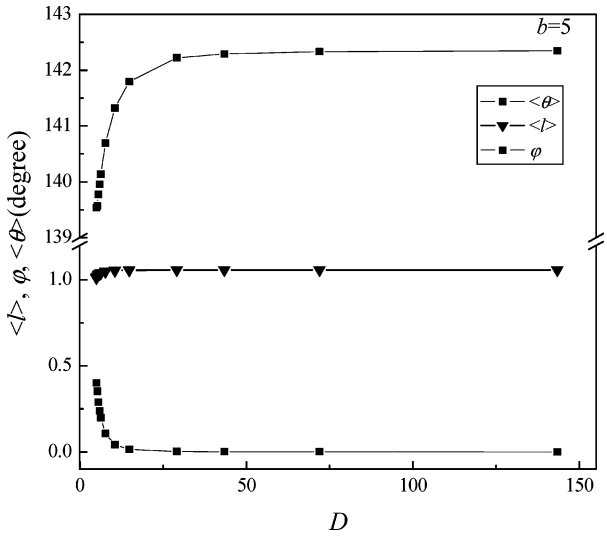

Figure 8. Variation of the mean valence angle $\langle \theta \rangle$, mean effective bond length $\langle l \rangle$, and volume fraction φ of a confined chain with the stiffness parameter $b = 5$ with the radius of confining sphere.

the sphere. We used the MC method to calculate this average to obtain $\langle R^2 \rangle = 1.2D^2$. Thus, the size ratio of a compact chain in a sphere is given as $\langle R^2 \rangle / \langle R_g^2 \rangle = 2$. This limit is almost reached in Figure 4 in semiflexible chains of $b = 20$ under strong spherical confinement. Interestingly, analogous calculations for a fully compacted random chain in a sphere with a concentric spherical hole gave the same size ratio 2.

The snapshot of the resulting structure of the stiff compressed chain is shown in Figure 9. The toroidal, donutlike structure is formed spontaneously in a spherical cavity. The chain is aligned along the internal walls of a sphere, and the central region remains quite empty. By reduction of chain stiffness, the tendency to form the toroidal (spool-like) structure diminishes, and the central hole is gradually filled up. In the WLC model of continuous elastic string, the toroidal structure can be considered as a consequence of string buckling. In the discrete model used in simulations, the chain contour adapts to the spherical confinement through adjustments of individual segments.

The data shown prove that semiflexible polymers can effectively be compacted into a sphere of radius of 1 or 2 orders

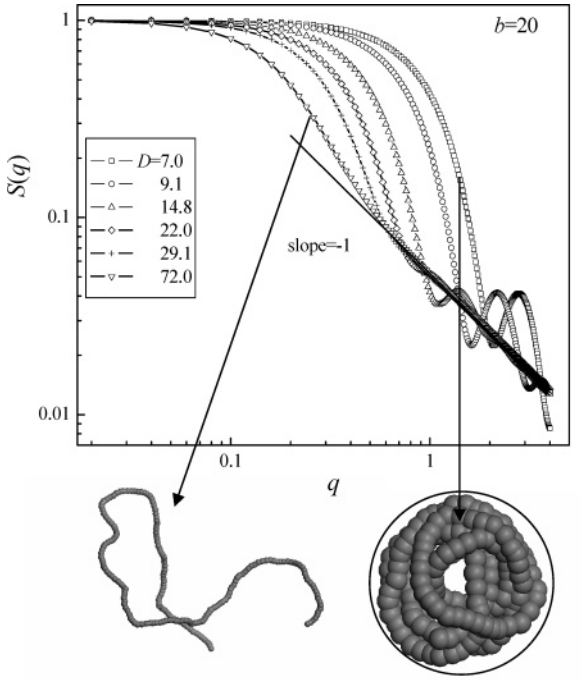

Figure 9. Logarithmic plot of the form factor for a chain with the stiffness parameter $b = 20$ confined in a spherical cavity of the radius D given in the legend as a function of the scattering wavevector. Snapshots exemplify the conformations of the free chain and of the spool-like chain confined at $D = 7$.

smaller than their persistence and contour lengths. The simulations of spherical confinement are highly relevant to various biological encapsulations of macromolecules in a spherical volume such as DNA packaging in a virus.[18] Recently, the predisposition of stiff chains to develop toroidal globules in spherical cavities was confirmed in experiments with actin filaments polymerized in vitro in emulsion droplets.[26] The fluorescent micrographs clearly show a heterogeneous distribution of actin filaments in small droplets with the dense layer (cortex) formed along the internal walls of droplets. On the contrary, a homogeneous distribution of actin filaments was observed[26] in large droplets. The cortex formation should be a consequence of toroidal arrangements of actin chains at high confinements in emulsion drops. Besides, the experiments[26] revealed that enhanced confinement induces the elastic stiffness of actin chains and networks relative to bulk properties. This observation is coherent with results[27] of isotropic elasticity simulations of semiflexible chains that have one end located in the origin and the other end constrained to the surface of sphere.

Scattering Structure Factors. Much useful information on internal structure of confined molecules can be obtained from the single-chain structure factor. The single-chain form factor $S(q)$ is defined in isotropic systems as

$$S(q) = \frac{1}{N^2} \left\langle \sum_{i=1}^{N} \sum_{j=1}^{N} \sin(qr_{ij})/qr_{ij} \right\rangle \tag{8}$$

where r_{ij} is the distance between segments i and j. The wavevector $q = 2\pi/x$ (x here is not reduced by l_0) was used in the range of x from about coil size to about monomer size. The comparison of simulation curves with the power-law functions $S(q) \sim q^{-1/\nu}$ (where ν is the exponent in the chain size scaling $R \sim N^{\nu}$ from the scaling theory)[6,28] gives hints on the chain shape in different regions of spatial dimensions and its alteration by confinement and may serve for the comparison with experimental results.

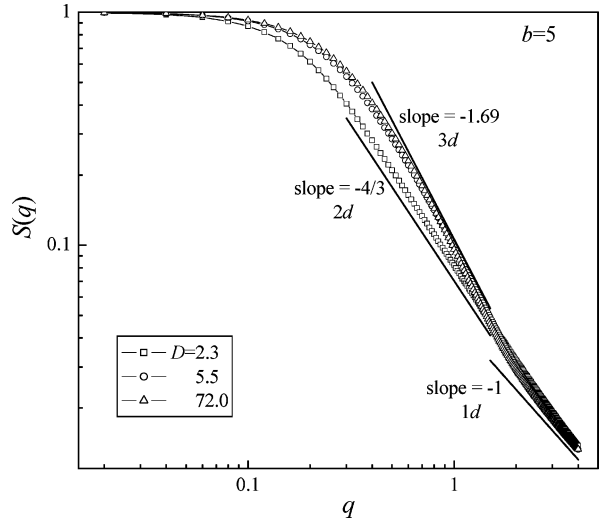

Figure 10. Logarithmic plot of the form factor of a chain with the stiffness parameter $b = 5$ confined in a slit of the half-width D given in the legend as a function of the scattering wavevector.

Log−log plots of the scattering form factors $S(q)$ of chains of $b = 5$ in a cylinder of radius D and in a slit of half-width D are shown in Figures 5 and 10, respectively. The straight lines next to the curves represent the slopes of the power-law predicted by the scaling theory.[6,28] Generally, up to three regimes discerned by the slopes of the computed scattering function can be recognized for uni- and biaxial confinements. The regime of a rigid rod (slope −1) is observable at high values of the wavevectors $ql_0 > 2\pi/P$ (on a local scale) in both types of confinements. The existence of an additional two regimes depends on the interplay of the P_{3D}, D, and R_g values. In the intermediate range of wavevectors of about $2\pi/P > ql_0 > 2\pi/2D$ associated with the organization of a chain within an individual blob of size $2D$, the slope −1.69, corresponding to a 3D coil in good solvent, is recognizable. The appearance of this regime assumes confinement that is not too strong, i.e., $P_{3D} < 2D$. The range of wavevectors of about $2\pi/2D > ql_0 > 2\pi/2R_g$ indicates the existence of the global structure of a confined polymer. This is the rodlike structure for a chain in a cylinder characterized by slope −1 and the 2D structure for a chain in a slit characterized by slope $-4/3$. This regime requires confinement that is not too weak, i.e., $D < R_g$. Thus, the stronger the confinement (smaller D), the smaller the scale of q covered by the intermediate regime and the larger the scale of q governed by the regime of global structure. In a very narrow tube, only one (Odijk) regime is observed at all wavevectors q, and the slope becomes very close to −1, the theoretical value for a rigid rod chain. Three regimes in the cylinder are linked to respective length scales of the chain structure in the snapshot in Figure 5. Similarly, in a slit of small half-width, the intermediate regime disappears, and only the regime describing a rigid rodlike chain at local scale and the regime describing a 2D chain at global scale are distinguished.

It is possible (at least semiquantitatively) to localize the transitions between three regimes and identify the transition with the physical properties in a cylinder. The first transition appears at high q. On decrease of q, the behavior of rigid rod, with slope −1, disappears, and this point represents the persistence length. For a broad cylinder, $D = 72.0$, this is observed at $q = 2\pi/x \cong 1.5$. The respective distance $x/l_0 \cong 6$ is close to the persistence length (eq 5) for a free chain of $b = 5$ as expected. In narrow cylinders, the transition shifts to higher q indicating a smaller local effective persistence length. The second transition between regimes appears at smaller value of q where the global rigid rodlike behavior of chain meets the more local behavior of a 3D blob of the size of a cylinder diameter. For $D = 5.5$, the transition is located at $q = 2\pi/x \cong 1$, and the respective distance $x \cong 6.3$ (size of blob) is relatively close to the cylinder diameter $2Dl_0 = 7.7$. For stronger confinement, this transition shifts to higher q reflecting the more extensive region of global persistence in the chain, and the position of transition indicates a smaller size of a 3D blob within the chain. In slits (Figure 10), the cross-overs between regimes are much more subtle than in cylinders.

Finally, in a sphere, the form factors $S(q)$ computed for confined chains of $b = 20$ show a complex structure (Figure 9). As confinement increases, the section of $S(q)$ at high q characterizing the local rodlike structure within the chain (with slope −1) starts to vanish, and a maximum appears instead. At the same time, at smaller q the slope of $S(q)$ turns from −1.69 to −3 (characteristic to a polymer globule) at intermediate confinements, or even to larger values at the strong confinement. The disappearance of a rigid structure at high q, however, does not mean that the local stiff character of the chain vanishes. Since the chain locally remains rigid (the valence angle decreases only slightly), this large change in $S(q)$ prompts another explanation. The snapshot picture, Figure 9, shows the densely packed organization of a stiff chain in sphere of $D = 7.0$. In compact structure, the local correlations between chain segments in the close vicinity spatially replace the correlations between segments along the chain backbone characteristic for a free chain. A similar trace of $S(q)$ but with weaker maximum shifted to larger wavevectors can be seen also for more flexible chains. The resulting $S(q)$ is thus a combination of effects of cavity walls and chain rigidity which organize together the chain conformation. Moreover, the snapshot, Figure 9, indicates a toroidal structure of a chain which, in order to decrease its bending, winds along the internal wall of a sphere and leaves even empty space in the center of the cavity. Interestingly, the reduced density in the center of a spherical cavity is not reflected in the change of the size ratio $\langle R^2\rangle/\langle R_g^2\rangle$ in Figure 4; the value is close to the limit $\langle R^2\rangle/\langle R_g^2\rangle = 2$. As mentioned earlier, this value is characteristic for a homogeneously compacted coil in spherical volume as well as to a compact coil with a concentric hole in the cavity.

Conclusions

In summary, we have demonstrated that molecular simulations are effective in providing the dimensional and structural quantities of semiflexible macromolecules in 1D, 2D, and 3D confinements. The discretized WLC chain model was used to calculate the persistence length, the chain dimensions, and the structure factors of polymers confined in slits, cylinders, and spheres. The transformation of the intrinsic persistence length of free chains into the apparent persistence length of confined chains was described for three restricting geometries. The qualitative differences in trends of the apparent persistence length and chain dimensions were observed between slits and cylinders on one side and spheres on the other side. For chain elongation in a cylinder, two different regimes (pertaining to strong and moderate confinements) and their crossover were identified and compared to predictions of scaling and Odijk theoretical models and to experimental observations. In a spherical cavity, the toroidal chain structure with a hole in the center was found under strong confinements.

The scattering form factor $S(q)$ computed for semiflexible confined chains reveals three different regimes of behavior in

a slit and a cylinder that match up well with the scaling theory arguments. The transition points between regimes fairly correlate with the physical quantities such as the persistence length and blob size. The complex form of the function $S(q)$ found for spherical confinement reflects the formation of toroidal chain structure. Qualitative agreement was found between the simulation results and experimental data for DNA molecules and actin filaments, confined in microfluidic channels and in spherical droplets, pertaining to the changes of the persistence lengths, chain elongation, and toroidal structure formation.

Acknowledgment. This work was supported by VEGA grants 2/6116/26 and 2/6014/26 and in part by the Center of Excellence COMCHEM.

References and Notes

(1) Zhou, H. X.; Dill, K. A. *Biochemistry* **2001**, *40*, 11289−11293.
(2) Chen, Y.-L.; Graham, M. D.; de Pablo, J. J.; Randall, G. C.; Gupta, M.; Doyle, P. S. *Phys. Rev. E* **2004**, *70*, 060901(R).
(3) Reisner, W. W.; Morton, K. J.; Riehn, R.; Wang, Y. M.; Yu, Z.; Rosen, M.; Sturm, J. C.; Chou, S. Y.; Frey, E.; Austin, R. H. *Phys. Rev. Lett.* **2005**, *94*, 196101.
(4) Köster, S.; Steinhauser, D.; Pfohl, T. *J. Phys.: Condens. Matter* **2005**, *17*, S4091−4104.
(5) Choi, M. C.; Santangelo, C. D.; Pelletier, O.; Kim, J. H.; Kwon, S. Y.; Wen, Z.; Li, Y.; Pincus, P. A.; Safinya, C. R.; Kim, M. W. *Macromolecules* **2005**, *38*, 9882−9884.
(6) Rubinstein, M.; Colby, H. *Polymer Physics*; Oxford University Press: New York, 2003.
(7) Cifra, P. *Polymer* **2004**, *45*, 5995−6002.
(8) Norisuye, T. *Prog. Polym. Sci.* **1993**, *18*, 543−584.
(9) Hendricks, J.; Kawakatsu, T.; Kawasaki, K.; Zimmermann, W. *Phys. Rev. E* **1995**, *51*, 2658−2661.
(10) Cifra, P. *J. Chem. Phys.* **2006**, *124*, 024706.
(11) Odijk, T. *Macromolecules* **1983**, *16*, 1340−1344.
(12) van Vliet, J. H.; Luyten, M. C.; ten Brinke, G. *Macromolecules* **1992**, *25*, 3802−3806.
(13) Cifra, P.; Bleha, T. *Macromol. Theory Simul.* **1999**, *8*, 603−610.
(14) Morrison, G.; Thirumalai, D. *J. Chem. Phys.* **2005**, *122*, 194907.
(15) Romiszowski, P.; Sikorski, A. *J. Math. Chem.* **2006**, *40*, 295−303.
(16) Brochard-Wyart, F.; Tanaka, T.; Borghi, N.; de Gennes, P.-G. *Langmuir* **2005**, *21*, 4144−4148.
(17) Tegenfeldt, J. O.; Prinz, C.; Cao, H.; Chou, S.; Reisner, W. W.; Riehn, R.; Wang, Y. M.; Cox, E. C.; Sturm, J. C.; Silberzan, P.; Austin, R. H. *Proc. Natl. Acad. Sci. U.S.A.* **2004**, *101*, 10979−10983.
(18) Kindt, J.; Tzlil, S.; Ben-Shaul, A.; Gelbart, W. M. *Proc. Natl. Acad. Sci. U.S.A.* **2001**, *98*, 13671−13613.
(19) Cifra, P.; Bleha, T. *Polymer* **2007**, *48*, 2444−2452.
(20) Milchev, A.; Binder, K. *Macromolecules* **1996**, *29*, 343−354.
(21) Fynewever, H.; Yethiraj, A. *J. Chem. Phys.* **1998**, *108*, 1636−1644.
(22) Riveline, D.; Wiggins, C. H.; Goldstein, R. E.; Ott, A. *Phys. Rev. E* **1997**, *56*, R1330−R1333.
(23) des Cloizeaux, J.; Jannink, G. *Polymers in Solutions: Their Modelling and Structure*; Clarendon: Oxford, 1990.
(24) Bishop, M.; Saltiel, C. J. *J. Chem. Phys.* **1988**, *88*, 6594−6596.
(25) Caccuito, A.; Luijten, E. *Nano Lett.* **2006**, *6*, 901−905.
(26) Claessens, M. M. A. E.; Tharmann, R.; Kroy, K.; Bausch, A. R. *Nat. Phys.* **2006**, *2*, 186−189.
(27) Cifra, P.; Bleha, T. *Macromol. Theory Simul.* **2007**, *16*, 501−512.
(28) de Gennes, P.-G. *Scaling Concepts in Polymer Physics*; Cornell University: Ithaca, NY, 1979.